Materials Today Sustainability 22 (2023) 100353

Contents lists available at ScienceDirect

Materials Today Sustainability

journal homepage: https://www.journals.elsevier.com/materials-today-sustainability

Carbon materials derived from cyano-based IL@ZIF-8 composites for CO_2 sorption separation systems

L.M. Esteves [a], T.J. Ferreira [a], A. Keba [a], J.M.S.S. Esperança [**], I.A.A.C. Esteves [*]

LAQV/REQUIMTE, Departamento de Química, Faculdade de Ciências e Tecnologia, Universidade NOVA de Lisboa, Caparica 2829-516, Portugal

ARTICLE INFO

Article history:
Received 20 January 2023
Received in revised form
1 February 2023
Accepted 6 February 2023
Available online 10 February 2023

Keywords:
CO_2 separation
Biogas upgrading
Zeolitic imidazolate framework-8 (ZIF-8)
Ionic liquids (ILs)
IL@MOF composites and derived carbons

ABSTRACT

The sorption capacity and selectivity of pre- and post-carbonized cyano-based metal-organic framework (MOF) composite materials (cyano-based IL@ZIF-8) were investigated for the first time. The influence of the ionic liquid (IL) loading and number of cyano groups in the IL anion on a materials gas sorption separation performance was studied. Sorption-desorption equilibrium isotherms of CO_2, CH_4, and N_2 were measured at 303 K in the ZIF-8, cyano-based IL@ZIF-8 composites and their derived carbon materials. The IL loading did not significantly affect the gas uptake of the carbon materials, while for the composites its main contribution was on the increase of the selectivity. The number of cyano groups in the anion played a key role in the sorption capacity and selectivity performance as it directly affects the N content and textural properties. The carbon material obtained from ZIF-8 (C_ZIF-8) precursor showed the best sorption capacity for all gases, just being surpassed by the C_15%[C_6MIM][$B(CN)_4$]@ZIF-8 carbon up to 1 bar. In terms of selectivity performance, carbons based on [C_6MIM][$B(CN)_4$]@ZIF-8 composites revealed to be equally or more selective than C_ZIF-8, increasing up to 65% between 0 and 1 bar depending on the mixture. The composites produced and their respective carbons demonstrated a promising application as sorbents for post-combustion CO_2 separation systems.

1. Introduction

The release of carbon dioxide (CO_2) to the atmosphere, the major greenhouse gas (GHG) contributing to climate change due to years of fossil fuels combustion, has led to serious environmental and energetic concerns [1]. To reduce GHGs emissions, new ways to slow the climate change impacts are needed to accomplish the emission policies imposed by the Paris Agreement [1–4]. Different strategies must be adopted to tackle the large amounts of emitted CO_2 and to gradually move towards a net-zero–CO_2–emissions economy. To accomplish that, fossil fuels replacement strategies [5] and the implementation of more carbon capture and storage (CCS) technologies, as well as the more recent carbon capture and utilization (CCU), are required [1]. Biomethane (bioCH_4) is considered a promising biofuel for natural gas replacement, and is obtained through biogas upgrading (a mixture consisting mostly of CO_2 and CH_4) [6,7]. Regarding CCS, post-combustion CO_2 capture/separation processes can be used to remove this gas from flue gas – a mixture mainly composed of nitrogen (N_2) and CO_2. Several technologies have been developed for this purpose, including chemical and physical solvent scrubbing, membranes, cryogenic distillation, and gas adsorption. Among them, chemical scrubbing using ethanolamines is the most mature one [8], but there are significant problems associated with the use of amines as a CO_2 absorbent material, like their volatility, absorbent degradation, high regeneration energy input, and equipment corrosion [9]. These drawbacks have propelled the development of new alternative technologies and materials to turn gas adsorption-based processes cost-competitive, as these systems are relatively simple and environmentally more favorable [10,11].

Adsorption-based gas processes have shown to be effective in both biogas upgrading and post-combustion CO_2 capture/separation [12]. There has been a growing and sustained effort to develop these adsorption systems, and they have shown potential to replace the conventional processes [12,13]. Even though some adsorption-based processes are well developed, i.e. pressure swing adsorption (PSA), the greatest research efforts have been focused on the

* Corresponding author.
** Corresponding author.
E-mail addresses: lm.esteves@fct.unl.pt (L.M. Esteves), tjo.ferreira@campus.fct.unl.pt (T.J. Ferreira), a.keba@campus.fct.unl.pt (A. Keba), jmesp@fct.unl.pt (J.M.S.S. Esperança), i.esteves@fct.unl.pt (I.A.A.C. Esteves).
[a] Equally contributing authors.

https://doi.org/10.1016/j.mtsust.2023.100353

adsorbent material. A wide range of adsorbent materials is reported almost daily [13,14]. The classical adsorbents (e.g. zeolites and activated carbon) and their derived materials have been extensively used. Meanwhile, metal-organic frameworks (MOFs) have emerged as a promising class of alternative adsorbents. MOFs are crystalline materials assembled by a coordination bond between an organic functional linker and a metal cation or small metallic clusters [15]. Their popularity in different fields of research is mainly due to their large surface area and pore volume, promising thermal and mechanical stabilities and structural arrangement that allows a finely tunable surface functionality [14,16–18].

The application of the large number of synthesized MOFs for adsorption-based CO_2 separation from other gases has been previously reviewed [18–20]. Therefore, adsorbent properties such as gas adsorption capacity or selectivity performance can be improved in MOFs. Post-synthesis modification strategies have been applied to modify their structures and are considered a step forward in MOF research [21]. In this regard, ionic liquids (ILs) impregnation to obtain IL/MOF composites (generically named as IL@MOF) [22–25] have shown a great potential in sorption-based gas separations [26,27]. This is due to the combination of high porosity and large surface area of MOFs with a high gas affinity of ILs, especially for CO_2 [22,28,29]. ILs are salts with organic, asymmetric cations and organic or inorganic anions with low melting points (below 373 K) and are usually defined as designer solvents [30]. Some of their inherent properties include negligible vapor pressure, non-flammability, high electrochemical and thermal stabilities as well as high CO_2 solubility [31]. Indeed, ILs have been considered as absorbent materials for some CO_2 post-combustion applications, but this is in an early stage and some issues like IL cost and degradation must still be addressed [13,32].

In the last 15 years, nanoporous carbon-based materials derived from MOFs have drawn increasing attention and hold promising potential in gas adsorption/separation applications [33,34]. MOFs are good candidates for templating materials given their high specific surface area, ordered porous structures, and tunable structural properties [35]. These carbons can be obtained by hard-templating [36–38] or via direct carbonization of the framework structures [37,39–41]. The first method uses porous solids as sacrificial scaffolds and a large quantity of organic or inorganic templates as carbon sources. In the final step, the template is removed using corrosive chemicals such as strong acids or aqueous alkali [42]. Interestingly, MOFs have enough carbon content so that they can be directly carbonized in a single-step procedure. Meanwhile, the final structure and properties of the MOF-derived porous carbons are influenced by the stability, chemical structure, and pore characteristics of their pristine MOF precursor. Thus, not only pristine MOFs can be carbonized but different MOFs-based materials, such as MOFs composites, have been considered to obtain porous carbons with enhanced adsorption properties [37]. Porous carbon materials rich in nitrogen (N) are highly desired in an attempt to enhance even more hydrogen-bonding interactions between the carbon surface and CO_2, promoting their adsorption capacity [43,44].

Like MOFs, ILs have been carbonized, but the obtained carbon materials present a low surface area and mostly mesoporosity and macroporosity [45], and therefore have been used in electrochemical applications [46]. There are a huge number of possible ILs-derived carbon materials owing to a large number of cation–anion possible combinations [46,47]. Nevertheless, not all ILs can be used as carbon precursors since many of them decompose into volatile compounds at high temperatures (>773 K) and, consequently, no/very low carbon yield is obtained. The low specific surface areas of the obtained carbons [48] are also pointed as a drawback for the application of ILs as carbon precursors. Reasonable carbon yields and structured carbon materials can be obtained by using ILs with nitrile/cyano groups [49,50], poly-ILs [51], and protic ILs [52]. These IL-based precursors have been considered for gas adsorption applications and can be used to produce N-doped carbons.

Herein, merging the best of the two research areas, the effect of direct carbonization of IL@MOF composites on the gas sorption uptake and, consequently, on their selectivity performance, was evaluated. The literature regarding the application of these composite carbon-derived materials is quite scarce, focusing its application in different research areas such as the H_2 uptake [45] and adsorption of organic molecules (liquid-phase adsorption) [53–56]. In this work, motivated by the good performance of cyano-based ILs as carbon precursors, three ILs ($[C_6MIM][N(CN)_2]$, $[C_6MIM][C(CN)_3]$, and $[C_6MIM][B(CN)_4]$) were impregnated in MOF ZIF-8 by direct-contact and then carbonized at 1273 K. MOFs containing zinc (Zn) in their structure, such as ZIF-8, are special for yielding potentially metal-free nanoporous carbons with a high specific surface area due to the low boiling point of Zn (~1180 K). The metal can be evaporated during the carbonization step, enhancing the material porosity. Moreover, ZIF-8 is itself an N-containing MOF due to its organic linker (that has 34 wt.% N content), and it can also contribute to the production of N-enriched nanoporous carbons [37]. The influence of the number of cyano groups in the anion (-CN) and the IL loading on the sorption capacity and selectivity performance of the resulting composites and carbon materials was investigated. Comparisons between the sorption capacity and selectivity of the pre- and post-carbonization IL@ZIF-8 composites were established. The characterization of all the materials was performed to evaluate the impact of the carbonization process in the chemical and crystalline structures of the materials, along with changes in the textural properties and morphology.

2. Materials and methods

2.1. Materials

MOF ZIF-8 (Basolite® Z1200, 2-methylimidazole zinc salt: $C_8H_{10}N_4Zn$) was purchased from Sigma-Aldrich, as produced by BASF SE. The ILs 1-hexyl-3-methylimidazolium dicyanamide ($[C_6MIM][N(CN)_2]$, 98%), 1-hexyl-3-methylimidazolium tricyanomethanide ($[C_6MIM][C(CN)_3]$, >98%) were acquired from IoLiTec GmbH, while 1-hexyl-3-methylimidazolium tetracyanoborate ($[C_6MIM][B(CN)_4]$, ≥98%) was acquired from Merck. All ILs were evacuated at 0.1 Pa and 323 K for 24–48 h. Acetone (99.8%, Carlo Erba) was used as a solvent for the preparation of IL@ZIF-8 composites. Potassium bromide (KBr, Merck) was used to prepare the sample tablets for Fourier transform infrared spectroscopy (FT-IR) analyses. Ethanol (99.9%, Scharlau) was used to disperse the samples for scanning transmission electron microscopy (STEM) imaging. All gases used in the sorption-desorption equilibrium measurements – N_2 (99.99%, also used in the carbonization of materials), CH_4 (99.95%), CO_2 (99.998%), and helium (He, >99%) were purchased from Praxair (Portugal).

2.2. Composites preparation

The preparation of IL@ZIF-8 composites followed the same experimental protocol reported in a previous work [22], where a 15 wt.% loading of $[C_2MIM][NTf_2]$ (9.3 mol.%) was considered as a reference. The molar ratio was kept constant for all ILs to establish valid comparisons between the produced composites. Additionally, a 30 wt.% loading of $[C_2MIM][NTf_2]$ (19.95 mol.%) was considered as another reference to study the IL loading effect. Once again, this molar ratio was kept constant for the produced composites with a higher IL loading.

Before the impregnation, the degassed IL was dissolved in acetone and stirred at room temperature for 15 min. This mixture was then added to a vial containing 1 g of degassed ZIF-8 (373 K for 3–4 h), followed by continuous stirring overnight at room temperature. To avoid acetone evaporation, the vial was capped while stirring. Afterward, the cap was removed and stirring was continued for 4–5 h at room temperature and then at 338 K for solvent evaporation. Finally, the composites were degassed at 373 K for 3–4 h. The obtained composites were named as x%[C_6MIM][$N(CN)_2$]@ZIF-8, x%[C_6MIM][$C(CN)_3$]@ZIF-8, and x%[C_6MIM][$B(CN)_4$]@ZIF-8, where x% corresponds to the IL mass loading (15 or 30 wt% equivalent content).

2.3. ZIF-8, ILs, and composites carbonization

Both pristine samples (ZIF-8 and ILs) and composites were carbonized in a quartz reactor placed in a horizontal furnace (Carbolite Gero EZS 1200) controlled by a PID programmable temperature controller (Eurotherm 3216). The sample was loaded in a boat-shaped crucible and placed in the center zone of the reactor, followed by a preheating step from room temperature to 373 K (with a ramping rate of 5 K/min), degassing the sample for 3–4 h. Then, the temperature was increased (5 K/min) up to 1273 K and kept at this temperature for 1 h and finally cooled down to room temperature. This allows for a fully degassed sample to be carbonized, and the chosen final temperature allows for the volatilization of zinc (Zn) given that the metal has a 'low' boiling point of 1180 K. The N_2 flow was maintained at 50 mL/min during all stages (heating and cooling). The obtained carbonaceous materials were named with the prefix 'C_', either for pristine samples or composites.

2.4. Materials characterization

Thermogravimetric analyses (TGA) were carried out on a thermogravimetric analyzer TA instruments model TGA Q50. Each sample was held on a platinum sample holder and was firstly heated at 373 K for 1 h to remove moisture or other pre-adsorbed impurities. Then the temperature was increased up to 1073 K with a heating rate of 2 K/min under a 50 mL/min flow of N_2.

Powder X-ray diffraction (PXRD) analyses were obtained in a Rigaku Miniflex II diffractometer using a monochromatic Cu-Kα radiation (λ = 1.540 Å) with an X-ray generator of 30 kV of voltage and 15 mA of current. XRD patterns were recorded in a 2θ range of 2–50°, with a scanning speed of 0.5°/min and a step width of 0.02°.

Infrared (FT-IR) spectra were acquired using a PerkinElmer FT-IR Spectrometer Spectrum Two model at room temperature between 4000 and 400 cm^{-1} and with a spectral resolution of 4 cm^{-1}. Neat ILs spectra were obtained with an attenuated total reflectance (ATR) module. The spectra of ZIF-8, IL@ZIF-8 composites, and carbonized samples required a transmission module, for which KBr pellets containing some milligrams of each sample were produced.

CNH elemental analyses were performed using an elemental analyzer Thermo Finnigan-CE Instruments Flash EA 1112 CHNS series. Replicate assays were performed for all materials, so the reported values were averaged.

A Micromeritics ASAP 2010 physisorption analyzer was used to perform N_2 sorption-desorption equilibrium at 77 K. Before the measurement, the samples were kept under vacuum for 3–4 h at 373 K. Textural properties, including Brunauer–Emmett–Teller(A_{BET}) and Langmuir ($A_{Langmuir}$) specific surface areas, total pore volume (V_p – at relative pressure p/p_0 of 0.95), and micropore volume ($V_{micropore}$), were obtained, along with the pore size distributions (PSDs – assuming a slit-shaped pores model) of the materials. Note that the micropore volume was calculated using the Dubinin-Astakhov equation, which is often used to determine the micropore volume of materials [57]. As for the PSDs, they were determined by non-local functional theory (NLDFT) calculations, which is the standard method recommended by the International Standard Organization (ISO) for a micropore and mesopore size analysis [58].

The surface features and morphology of the samples were investigated by a Hitachi UHR-STEM HD2700 type B model microscope, with an acceleration voltage of 200 kV. A few milligrams of each sample were dispersed in ethanol and then two drops of the resulting suspension were deposited on a carbon-coated copper grid (300 mesh), which was finally dried at room temperature. Scanning electron microscopy (SEM) and transmission electron microscopy (TEM) imagings were obtained at different magnifications, ranging between 30 k x to 150 k x.

2.5. Gas sorption-desorption equilibria of CO_2, CH_4, and N_2

The CO_2, CH_4, and N_2 sorption-desorption equilibria were experimentally determined using a standard static gravimetric method between 0 and 10 bar, at 303 K. For this purpose, it was used a gravimetric unit that includes a high accuracy ISOSORP 2000 magnetic-suspension balance (Rubotherm GmbH), with a resolution of 10^{-5} g, uncertainty ≤0.002%, and reproducibility $\leq 3 \times 10^{-5}$ g. The temperature inside the unit is controlled using an accurate F32-HL (Julabo GmbH) refrigerating/heating circulator (±0.1 K), and the pressure is measured using a parallel set of pressure transducers: Baratron model 627D (MKS Instruments GmbH, accurate to 0.12% of the measured value) for 0–1 bar, and Omegadyne Inc. models PX01C1-150A5T and PX01C1-500A5T (both accurate to 0.05% of full scale) for 0–10 bar and 0–35 bar, respectively. The pressure was recorded and monitored using in-house developed software. The samples (0.3–0.4 g) were degassed *in situ* at 373 K for 3–4 h and then conditioned overnight to 303 K under vacuum. The detailed information about the gravimetric unit and methodology employed in the measurements can be found in our previous works [14,22,59].

The specific net adsorption quantity (q_{net}), expressed in moles of adsorbed gas per unit mass of adsorbent, is used to report adsorption data. Moreover, reporting in q_{net} avoids drawbacks related to the use of probe molecules for the determination of the reference state [60]. Considering a gravimetric experiment, q_{net} is given by Eq. (1)

$$q_{net} = \frac{m - m_s - m_h + V_h\,\rho_g}{m_s\,M_w}, \tag{1}$$

where m is the weighed mass registered by the balance, m_s is the mass of the (degassed) solid in the sample holder, m_h and V_h are the total mass and volume of all parts of the sample holder contributing to buoyancy effects, respectively; ρ_g is the gas density at the equilibrium pressure and temperature of the measurement and M_w is the molecular weight of the measured gas. The excess adsorption quantity (q_{exc}), expressed in moles of adsorbed gas per unit mass of adsorbent, is reported in Eq. (2) as

$$q_{exc} = q_{net} + V_s\rho_g, \tag{2}$$

where V_s is the specific volume of the adsorbent impenetrable to the adsorbate molecules ($V_s = 1/\rho_S$) and ρ_S is the solid matrix density, estimated by He pycnometry. It was decided to present sorption-desorption data in excess rather than in total quantity (q_t), the most often-used quantity to report the sorbed amount and in process modeling, since the total pore/micropore volume of the [C_6MIM][$B(CN)_4$]-containing carbons could not be determined [61].

Eq. (2) is also applicable when a porous solid is impregnated with an IL, provided that ρ_S is corrected for the presence of the IL. Helium (He) pycnometry measurements were performed using the abovementioned gravimetric apparatus at 333 K, in which He is considered an inert probe molecule that penetrates all the accessible pore volume of the material without being adsorbed.

Excess sorption-desorption isotherms of CO_2, CH_4, and N_2 gases were fitted to the Sips adsorption isotherm model (Eq. (3)) [58] as follows:

$$q_{exc}(P) = \frac{q_s (bP)^{1/n}}{1 + (bP)^{1/n}} \quad (3)$$

where q_s is the maximum adsorbed amount, P is the pressure, b is the affinity parameter, and n corresponds to the heterogeneity parameter. Note that in this work, the term sorption includes both adsorption and absorption phenomena.

The ideal CO_2/CH_4 and CO_2/N_2 selectivities were determined by Eqs. (4) and (5), respectively, considering the partial pressure of the gases in different hypothetical mixtures of interest (50:50 CO_2/CH_4, 50:50 CO_2/N_2, 40:60 CO_2/CH_4, and 15:85 CO_2/N_2) and using the parameters obtained from Sips fittings.

$$S_{CO_2/CH_4} = \frac{q_{CO_2}}{q_{CH_4}} \quad (4)$$

$$S_{CO_2/N_2} = \frac{q_{CO_2}}{q_{N_2}} \quad (5)$$

3. Results and discussion

3.1. Materials characterization

To proceed with the carbonization of ZIF-8, ILs, and IL@ZIF-8 composites, the evaluation of their thermal stability was carried out by TGA. The obtained thermograms are shown in Fig. 1. The ZIF-8 thermogram remains constant until 690 K, after which the weight loss gradually increases due to the decomposition of its organic linker [62]. Neat cyano-based ILs showed two decomposition stages: the first one is related to the decomposition of the imidazolium cation and the second one is consistent with the degradation of the anion [63,64]. The thermograms of the composites presented two steps of weight loss assigned to the IL decomposition and the decomposition of the organic linkers of ZIF-8, respectively.

The starting decomposition temperature (T_{start}) of the materials, which corresponds to the temperature at which the sample reaches 1 wt.% of weight loss, is shown in Table S1 (See Supporting Information, SI). Comparing the T_{start} of neat ILs, it was observed that when the number of cyano groups rises, the T_{start} increases. Both the number of cyano groups and IL loading had an impact on the T_{start} of the composites. All composites possess lower T_{start} than their respective neat IL, meaning that the degradation of composites is slightly faster than that of the pure IL or ZIF-8. For IL@ZIF-8 materials with a 15 wt.% IL equivalent loading, a gradual increase in the difference between the T_{start} of neat IL and the respective composite with the increase of cyano groups was also observed. These differences were 4 K, 18 K, and 49 K for 15%[C_6MIM][$N(CN)_2$]@ZIF-8, 15%[C_6MIM][$C(CN)_3$]@ZIF-8, and 15%[C_6MIM][$B(CN)_4$]@ZIF-8, respectively. The increase of the IL loading led to a lower T_{start}, exception made for [C_6MIM][$C(CN)_3$]-containing composites.

The calculated TGA profiles for IL@ZIF-8 composites were determined using the decomposition profiles of their neat precursors and the impregnated IL loading, as revealed by Eq. (6)

$$\text{Calc. wt.\%}|_T = \text{wt.\%}_{ZIF-8}|_T \times (1 - \text{wt.\% loading}_{IL}) + \text{wt.\%}_{IL}|_T \times \text{wt.\% loading}_{IL} \quad (6)$$

There is a higher thermal degradation rate than expected since the composite TGA profiles shifted to lower temperatures than the calculated ones. These results suggest the existence of direct and specific IL-MOF interactions that affect the thermal stability of ZIF-8 by accelerating its degradation.

X-ray diffractograms of ZIF-8, cyano-based IL@ZIF-8 composites, and their respective carbon materials are depicted in Fig. 2. The ZIF-8 diffractogram is in accordance with the literature [65]. The characteristic peaks of ZIF-8 remain intact after IL impregnation, which means that there was no change in the crystalline structure of ZIF-8 upon IL impregnation. As PXRD data were normalized, it was possible to detect changes in the intensity of some diffraction peaks after IL incorporation, especially those at 16.6° and 18.1°. Apart from the sample preferred orientation, instrument alignment, sample decomposition, or composite preparation that can affect the intensity, this trend can be attributed to a change in the electronic density of the MOF caused by the presence of the IL [23,29]. The PXRD patterns of the as-produced carbon materials showed broad peaks at approximately 26°, which is assigned to the (002) diffraction plane of graphitic carbon [45]. This indicates that the carbonization process led to a crystallinity loss. Moreover, as the IL loading increases, a slight increase in the intensity of this peak, which is related to an increase in the amount of the amorphous phase, was observed [66].

The FT-IR spectra of composites (*See* SI, Fig. S1) revealed the presence of the IL upon the structure of the MOF, as both ZIF-8 bands and those related to the IL were observed in the composites spectra [67,68]. The characteristic IL bands of −C≡N stretching vibrations were observed at 2127, 2154, and 2222 cm^{-1} for neat [C_6MIM][$N(CN)_2$], [C_6MIM][$C(CN)_3$], and [C_6MIM][$C(CN)_4$], respectively [69]. Except for [C_6MIM][$B(CN)_4$]-containing composites, the position of these bands shifted after the IL incorporation. Blue shifts of 13 cm^{-1} and 8 cm^{-1} were observed for [C_6MIM][$N(CN)_2$]- and [C_6MIM][$C(CN)_3$]-containing composites, respectively, reaffirming the existence of specific interactions between the IL and ZIF-8. Regarding the FT-IR spectra of the obtained carbon materials, several bands related to the presence of N were observed. The stretching bands at around 1185 and 1116 cm^{-1}, 1380 cm^{-1}, and 1570 cm^{-1} are assigned to C−N (sp^3), C=N (sp^2), and C=N, or N−H groups, respectively [54,55,70,71]. This confirms that the produced carbons have N-containing groups in their structure.

The textural properties of the adsorbents used in this study, including total pore volume (V_p), micropore volume ($V_{micropore}$), Brunauer−Emmett−Teller, and Langmuir specific surface areas (A_{BET} and $A_{Langmuir}$, respectively), are given in Table 1. The N_2 isotherms from which these properties were calculated, as well as the PSDs derived from NLDFT calculations, are shown in the supplementary information (*See* SI, Figs. S2 and S3). The results obtained for ZIF-8 are following those described in the literature [39,72]. Regarding the composites, the textural properties decreased after the IL incorporation [68,73]. A decrease in the textural properties with both the increase of the IL loading and the number of cyano groups was observed. Except for [C_6MIM][$B(CN)_4$]-containing composites, the other composites presented similar results among the samples with the same molar amount of IL impregnated. For example, the A_{BET} of 15%[C_6MIM][$N(CN)_2$]@ZIF-8 and 30%[C_6MIM][$N(CN)_2$]@ZIF-8 were 38% and 69% lower than the A_{BET} of pristine ZIF-8, respectively. Furthermore, the A_{BET} of 15%[C_6MIM][$C(CN)_3$]

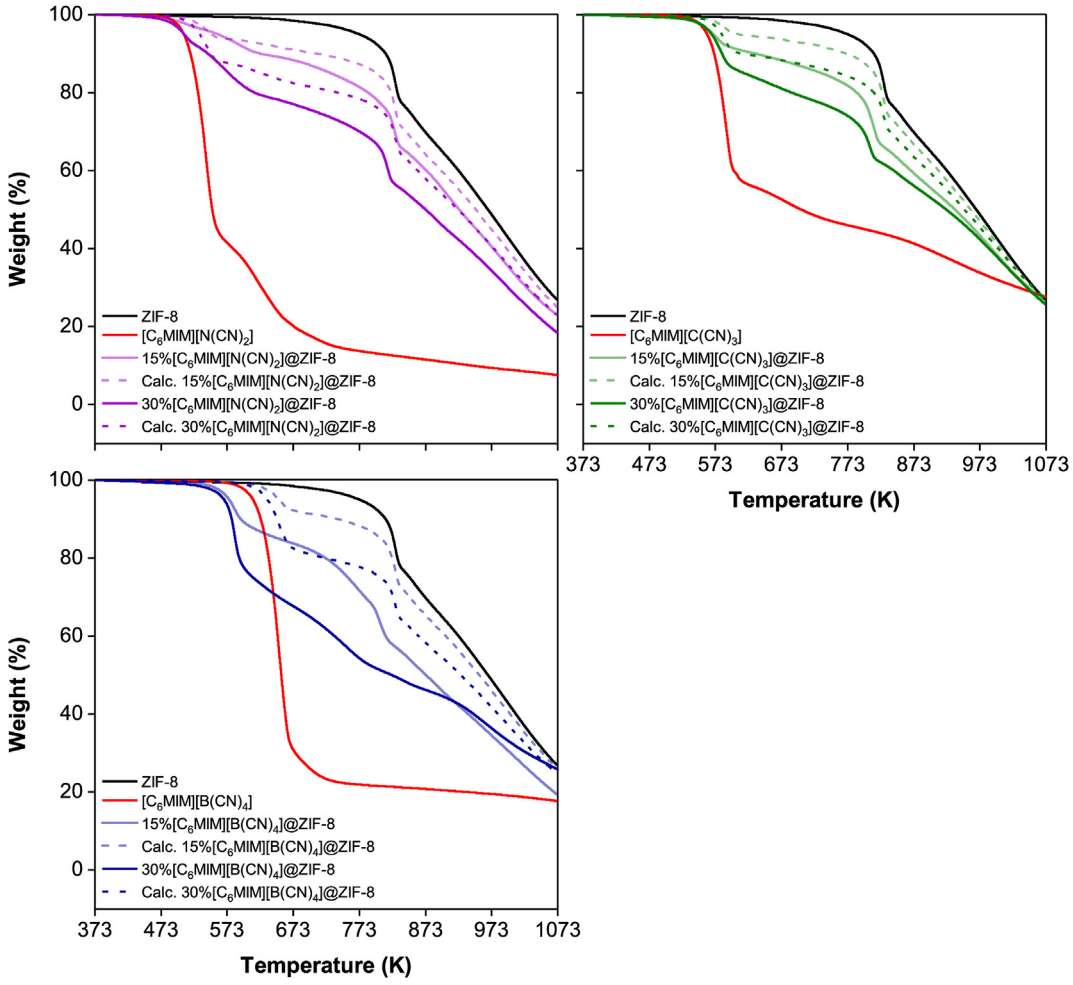

Fig. 1. Thermogravimetric analysesthermograms of ZIF-8, cyano-based ILs, and cyano-based IL@ZIF-8 composites.

@ZIF-8 and 30%[C_6MIM][C(CN)$_3$]@ZIF-8 were, respectively, 39% and 77% lower than the A_{BET} of pristine ZIF-8. According to the IUPAC classification [74], the obtained isotherms (*See* SI, Fig. S2) are Type I [74], suggesting the dominance of microporous characteristics on pristine ZIF-8 and on [C_6MIM][N(CN)$_2$]- and [C_6MIM][C(CN)$_3$]-containing composites. No hysteresis was observed and, thus, these materials are completely reversible. The textural properties of the composites were also determined on an IL-free basis, i.e. per gram of ZIF-8 (values in brackets on Table 1), which indicate a pore occupation/blockage by the IL as the IL-free textural properties are lower than those of pristine ZIF-8.

All samples containing [C_6MIM][B(CN)$_4$] (both composites and carbons) showed an unexpected trend. As already reported in our previous study [61], the N_2 sorption-desorption isotherms for [C_6MIM][B(CN)$_4$]-containing composites were Type II isotherms, a characteristic of non-porous materials. This justifies the obtained textural properties for this IL-containing samples. It has been observed that the interaction of the $[B(CN)_4]^-$ anion with the imidazolate linker of ZIF-8 seems to tune the material flexibility effect and directly affect the performance of ZIF-8 under N_2 sorption-desorption measurements at 77 K.

The carbonization of cyano-based ILs provided very low and/or non-defined surface area carbons (Table 1 and Fig. S2 in SI). This was expected as ILs do not present a well-defined structure. Comparing with its precursor, C_ZIF-8 presented lower textural properties. This is due to the partial collapse of the ZIF-8 structure during carbonization that consequently resulted in a pore size range modification [39] towards a more mesoporous carbonaceous material with some ultramicroporosity.

Interestingly, contrary to the composite materials, the IL loading increase did not affect the textural properties of the cyano-based IL@ZIF-8 carbons [55]. The high-loading (30 wt.% equivalent) IL@ZIF-8 carbons showed a higher specific surface area and total pore volume than their precursors (Fig. 3). Regarding the number of cyano groups, it was observed that carbon materials followed the same trend of their precursor composites: increased cyano groups led to the reduction of the textural properties. The isotherms of the resulting carbons (*See* SI, Fig. S2) are a mix of Types I and IV, with an H4 hysteresis at a relative pressure between 0.4 and 0.9, thus indicating the presence of both small micropores and mesopores [74]. It has been noticed that carbons containing both [C_6MIM][N(CN)$_2$] and [C_6MIM][C(CN)$_3$] have a more noticeable mesoporosity, which increases with the increase of IL loading. Their pore size distribution (*See* SI, Fig. S3) showed a high portion of small micropores, i.e. pores lower than 10 Å, derived from the framework collapse and graphitization and also a significant portion of pores between 10 and 20 Å. Besides, the composites with a higher IL loading showed an increase in the pore width (>20 Å) due to the generated mesoporosity.

The elemental analysis of the composites (Table 1) showed N enrichment after IL impregnation, and the experimental results were very close to the theoretical ones. After carbonization, the N

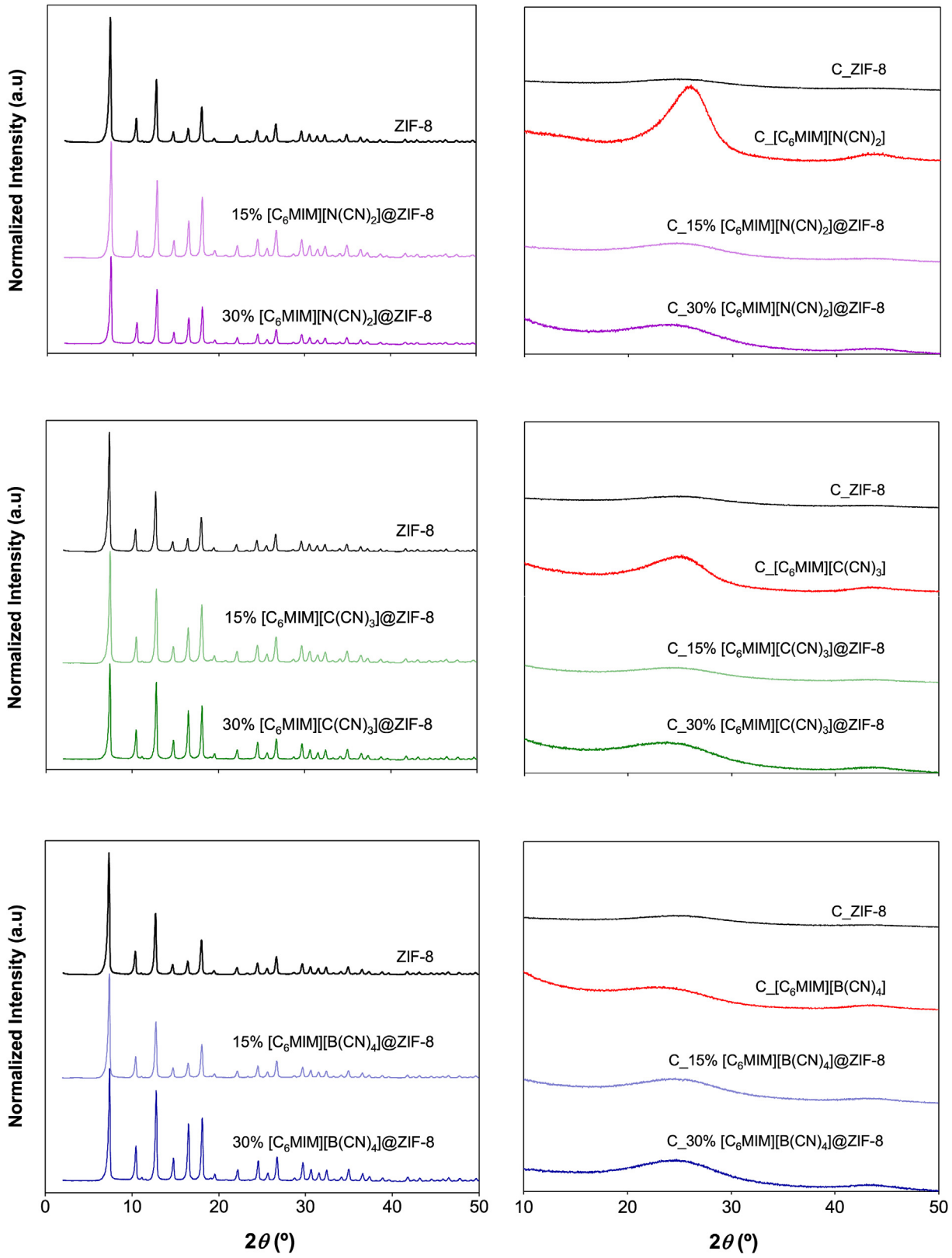

Fig. 2. Normalized powder X-ray diffraction patterns of ZIF-8, cyano-based IL@ZIF-8 composites, and their respective carbon materials.

Table 1
Textural properties of the adsorbents used in this study, obtained by N_2 physisorption at 77 K and He pycnometry and nitrogen content.

Sample	V_p[a] (cm^3/g)	$V_{micropore}$[a] (cm^3/g)	A_{BET}[a] (m^2/g)	$A_{Langmuir}$[a] (m^2/g)	ρ_s (g/cm^3)	N content[b] (wt.%)
ZIF-8	0.666	0.656	1862	1926	1.49	23.6 (24.6)
C_ZIF-8	0.372	0.352	755	855	1.91	8.0
15%[C_6MIM][$N(CN)_2$]@ZIF-8	0.422 (0.466)	0.415 (0.459)	1148 (1269)	1185 (1308)	1.32	25.0 (25.1)
30%[C_6MIM][$N(CN)_2$]@ZIF-8	0.226 (0.284)	0.218 (0.274)	568 (714)	584 (734)	1.25	25.5 (25.7)
C_[C_6MIM][$N(CN)_2$]	0.010	0.002	2	3	1.73	10.5
C_15%[C_6MIM][$N(CN)_2$]@ZIF-8	0.329	0.315	724	809	2.02	7.7
C_30%[C_6MIM][$N(CN)_2$]@ZIF-8	0.354	0.323	754	803	2.26	7.2
15%[C_6MIM][$C(CN)_3$]@ZIF-8	0.403 (0.450)	0.396 (0.442)	1101 (1229)	1137 (1269)	1.32	26.1 (24.9)
30%[C_6MIM][$C(CN)_3$]@ZIF-8	0.156 (0.200)	0.148 (0.190)	389 (499)	401 (514)	1.23	25.3 (25.2)
C_[C_6MIM][$C(CN)_3$]	0.000	0.000	3	3	1.66	7.3
C_15%[C_6MIM][$C(CN)_3$]@ZIF-8	0.321	0.300	669	756	2.01	7.6
C_30%[C_6MIM][$C(CN)_3$]@ZIF-8	0.353	0.313	701	746	1.95	6.6
15%[C_6MIM][$B(CN)_4$]@ZIF-8	0.005 (0.006)	0.002 (0.002)	5 (6)	5 (6)	1.27	24.9 (25.2)
30%[C_6MIM][$B(CN)_4$]@ZIF-8	0.003 (0.004)	0.001 (0.001)	2 (3)	2 (3)	1.28	26.3 (25.8)
C_[C_6MIM][$B(CN)_4$]	n.d	n.d	n.d	n.d	1.59	20.0
C_15%[C_6MIM][$B(CN)_4$]@ZIF-8	n.d	n.d	n.d	n.d	1.99	8.5
C_30%[C_6MIM][$B(CN)_4$]@ZIF-8	n.d	n.d	n.d	n.d	2.14	10.6

[a] The values in brackets correspond to the textural properties on an IL-free basis, expressed per gram of ZIF-8. Note that n.d stands for 'not determined'.
[b] The values in brackets correspond to the theoretical N composition.

content of the resulting carbon materials was lower than their precursors. This was expected, as the carbonization of some materials means the volatilization of functional groups, along with an increase in the carbon content. The N content of the obtained carbon materials strongly depends on ILs containing N species [75]. The carbon materials derived from [C_6MIM][$B(CN)_4$]-containing composites presented a higher N content than C_ZIF-8. C_[C_6MIM][$B(CN)_4$] showed the highest N content (20.0 wt.%) among all the prepared carbon materials. Consequently, both C_15%[C_6MIM][$B(CN)_4$]@ZIF-8 and C_30%[C_6MIM][$B(CN)_4$]@ZIF-8 presented N contents of 8.5 and 10.6 wt.%, respectively. These values are consistent with those usually observed in the literature for carbons obtained at similar carbonization conditions and derived from composites with the IL composed by $[B(CN)_4]^-$ anion [45]. The [C_6MIM][$N(CN)_2$]- and [C_6MIM][$C(CN)_3$]-containing carbons showed similar elemental compositions with N contents around 7 wt.%.

The surface morphology of the synthesized carbons was investigated by STEM, and the obtained images were compared with those of pristine ZIF-8 and composites (Fig. 4). The SEM and TEM images of pristine ZIF-8, 15%[C_6MIM][$N(CN)_2$]@ZIF-8, and 15%[C_6MIM][$C(CN)_3$]@ZIF-8 can be found elsewhere [22]. It was observed that upon IL impregnation, ZIF-8 crystals tend to be more rounded while preserving their crystalline structure. This trend was also observed on carbonized samples. The representative SEM and TEM images for C_ZIF-8, C_15%[C_6MIM][$N(CN)_2$]@ZIF-8, and C_30%[C_6MIM][$N(CN)_2$]@ZIF-8 are in Fig. 4 and S4–S6 (See SI). Fig. 4 (a) revealed that C_ZIF-8 became slightly more rounded but has a similar crystalline shape and surface morphology than pristine ZIF-8 [39]. Compared with C_ZIF-8, the carbonized composites are

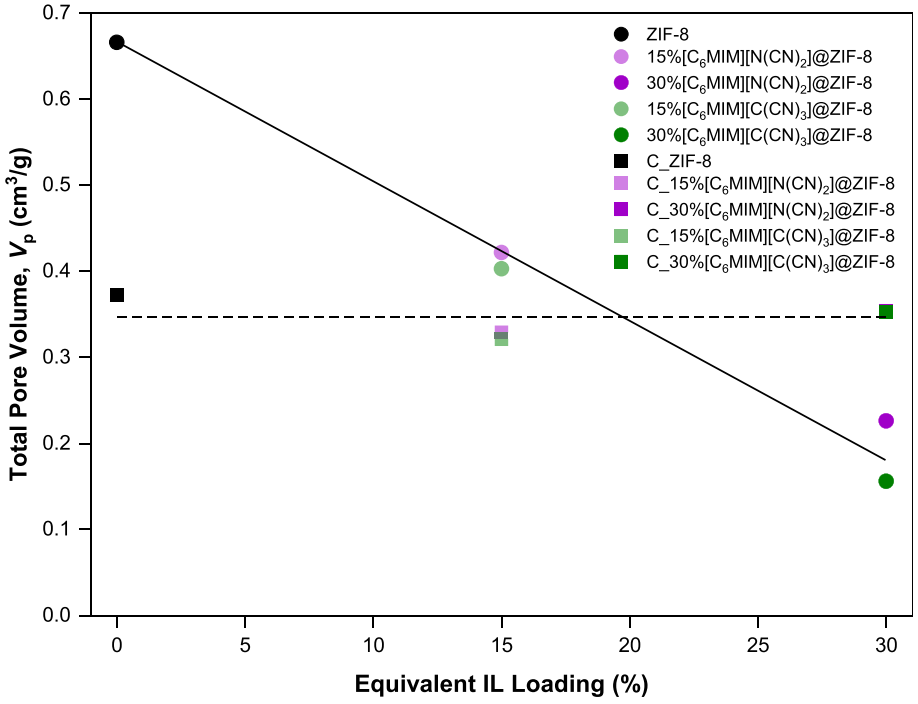

Fig. 3. Influence of the IL loading on the total pore volume of the produced IL@ZIF-8 composites and their respective carbons. The lines are guide-to-the-eye.

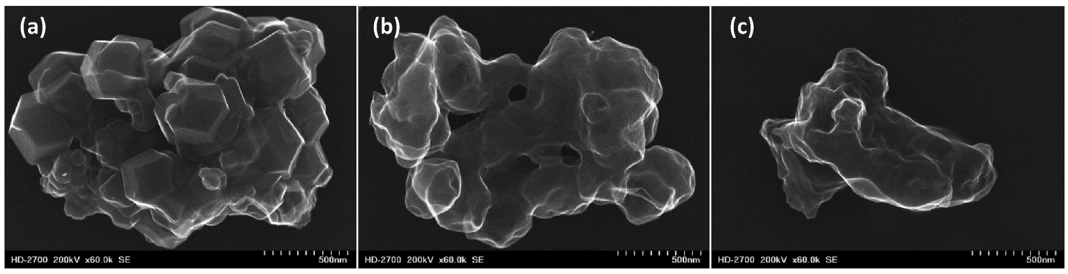

Fig. 4. Scanning electron microscopy images of (a) C_ZIF-8, (b) C_15% [C_6MIM][N(CN)$_2$]@ZIF-8 and (c) C_30% [C_6MIM][N(CN)$_2$]@ZIF-8 (scale bar: 500 nm; magnification: ×60 k).

more rounded and this effect is more prominent with the increase of the IL loading (Fig. 4(b) and (c)).

3.2. Sorption performance of the cyano-based IL@ZIF-8 composites and their derived carbons

Single-component CO_2, CH_4, and N_2 sorption-desorption equilibrium isotherms were measured at 303 K in the ZIF-8, cyano-based IL@ZIF-8 composites, and their derived carbon materials (Fig. 5 and Fig. S7, and Tables S2–S8 in SI). The sorption isotherms are reported in excess sorption quantity and were fitted using the Sips model (Eq. (3)). The parameters that describe the adsorbent-absorbate systems obtained from the prediction by the Sips equation with the experimental data are presented in Table S9 (See SI). The highest maximum adsorbed quantities (q_s) were observed for ZIF-8 and C_ZIF-8. For all gases, the parameter n, which characterizes the system heterogeneity, is lower than unity for composites. In the case of carbon materials, n is greater than one, indicating some degree of heterogeneity in those systems. The affinity factor, b, is higher in CO_2, suggesting that CO_2 is more attracted to the sorbent surface. Still, b values are all close to zero, indicating that the gases studied herein are weakly attracted.

As can be seen in Fig. 5, among the three gases, CO_2 was adsorbed the most due to its significant quadrupole moment [76].

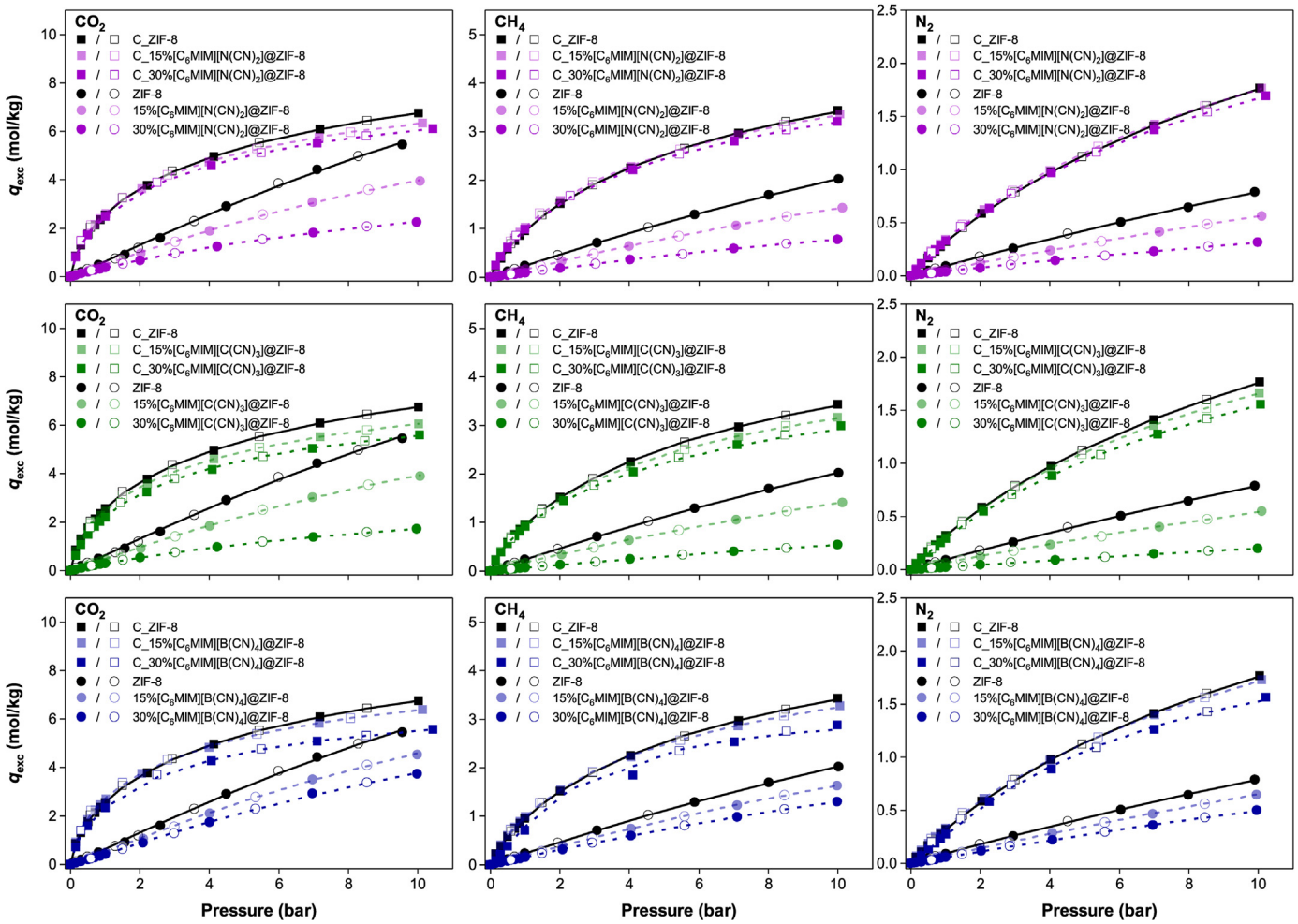

Fig. 5. Single-component sorption-desorption equilibrium isotherms of CO_2, CH_4, and N_2 in pristine ZIF-8, cyano-based IL@ZIF-8 composites and their respective derived carbons at 303 K. Closed and open symbols denote the sorption and desorption data, respectively. Lines represent the Sips sorption isotherm model fitting to the experimental data points.

Table 2
Comparison of the CO_2 (low-pressure regime) and CH_4 (high-pressure regime) adsorption capacity of the herein produced carbon materials with commercial and biomass-derived activated carbons.

Sample	CO_2 sorption capacity (mol/kg)	CH_4 sorption capacity (mol/kg)	Reference
Maxsorb III activated carbon	1.3 (0.5 bar, 300 K)	5.9 (10.0 bar, 300 K)	[78]
NORIT R1 Extra activated carbon	1.4 (0.5 bar, 298 K)	4.0 (9.7 bar, 298 K)	[79]
BPL activated carbon	1.0 (0.5 bar, 298 K)	3.1 (12.9 bar, 301 K)	[80,81]
ANGUARD 5 activated carbon	1.0 (0.5 bar, 290 K)	3.9 (11.8 bar, 298 K)	[82]
MCW(PA)3 h activated carbon	1.3 (0.4 bar, 303 K)	3.5 (10.3 bar, 303 K)	[83]
C_ZIF-8	1.8 (0.5 bar, 303 K)	3.4 (10.0 bar, 303 K)	This work
C_15%[C_6MIM][$B(CN)_4$]@ZIF-8	1.8 (0.5 bar, 303 K)	3.3 (10.0 bar, 303 K)	This work

The experimentally obtained isotherms are all Type I, according to the IUPAC classification [74]. Comparing the isotherms of ZIF-8 with those obtained for cyano-based composites, it was observed that upon IL impregnation and with the increase of the IL loading, the CO_2, CH_4, and N_2 uptakes decrease as a consequence of the lower specific surface area and total pore volume of the composites. It has already been demonstrated [22,68] that the presence of IL is the sole responsible for the lower obtained sorption capacities because no structure changes were observed upon IL impregnation. Herein, at moderate-to-high pressures, all composites presented lower sorption capacities compared to ZIF-8 due to the decrease of the pore volume by the presence of the IL (Table 1), since the total pore volume is the dominant factor governing the adsorption uptake in this pressure region. Likewise, at a low pressure (0–1 bar), all composites showed lower sorption capacities than pristine ZIF-8 (*See* SI, Fig. S7), meaning that the interactions between MOF, IL, and the sorbed gas, which are dominating at this pressure range, are not strong enough to surpass the loss of sorption sites [22,68]. Increasing the IL loading did not have a positive effect on the sorption capacities as the composites with equivalent 30 wt.% showed a lower gas uptake than those with 15 wt.%. This is due to the significant loss of the textural properties of high-loading composites. Thus, independently of the IL loading, cyano-based composites exhibited the descending order of the anions in terms of the CO_2 sorption capacity $[B(CN)_4]^- > [N(CN)_2]^- > [C(CN)_3]^-$.

The carbon materials derived from ZIF-8 and cyano-based IL@ZIF-8 composites showed higher uptakes for all studied gases (Fig. 5) than ZIF-8 and their respective composites. The obtained isotherms are Type I (b), which are usually found in materials possessing a pore size distribution from wider micropores and narrow mesopores [74]. This is the case of carbon materials whose isotherms are more concave to the pressure axis as a consequence of the carbonization step that affects the material porosity. The IL-derived carbons did not adsorb in all pressure ranges, which is related to their non-porous structure.

It has been stated that both N content and textural properties play a key role in the CO_2 uptake [45,77]. At moderate-to-high pressures, the CO_2 sorption capacity corresponded well with carbon materials porosity characteristics, i.e. the CO_2 uptake shows almost a linear dependence with the pore volume. However, it was observed that at these pressures the pore volume, in some cases, is not the only influencer on the CO_2 sorption capacity. For example, the textural properties of C_15%[C_6MIM][$B(CN)_4$]@ZIF-8 could not be determined, but this was the carbon with the second highest N content. This material showed a CO_2 uptake closer to C_ZIF-8 than C_15%[C_6MIM][$N(CN)_2$]@ZIF-8, and C_15%[C_6MIM][$C(CN)_3$]@ZIF-8, and these last two carbons have a lower N content. These results suggest that the N-content can increase the sorption capacity. Given the N_2 sorption-desorption at 77 K data of [C_6MIM][$B(CN)_4$]-containing materials, it was not expected that these composites could adsorb in the same magnitude or even higher than the composites investigated in our previous works [22,25,68]. The same rationale is applied to their-derived carbons as their textural properties could not be determined, and therefore they should not be good adsorbents.

At the low-pressure range, a stronger interaction of CO_2 with N-rich carbon materials (See SI, Fig. S7) was confirmed. C_15%[C_6MIM][$N(CN)_2$]@ZIF-8 showed almost the same sorption capacity as C_ZIF-8, and C_15%[C_6MIM][$B(CN)_4$]@ZIF-8 was able to surpass it as a consequence of its higher N content. Once again, the carbon materials derived from high IL loading composites showed a lower sorption capacity at all pressure range for the three gases studied. The above-mentioned results indicate that both the N content and textural properties are governing the CO_2 sorption capacity.

Table 2 compares the CO_2 and CH_4 sorption capacities of commercial and biomass-derived activated carbons reported in the literature, with some carbon materials produced herein. It can be observed that the produced materials show 29–80% increase in the CO_2 adsorption capacity at 0.5 bar, when compared to other activated carbons, confirming the potential of these materials for a low-pressure (post-combustion) CO_2 separation. In terms of high-pressure applications like CH_4 storage, other carbon materials like Maxsorb III should be preferred. It should be noted that the adsorption data of the activated carbons presented in Table 2 are in the total sorption quantity, unlike the data herein that were reported in the excess sorption quantity. This means that comparisons between materials for CO_2 are valid as excess and total quantities are very similar at low pressures (0.4–0.5 bar). For CH_4, as comparisons are drawn in the high-pressure regime, the values for C_ZIF-8 and C_15%[C_6MIM][$B(CN)_4$]@ZIF-8 are slightly undervalued.

Fig. 6 shows the calculated ideal CO_2/CH_4 and CO_2/N_2 selectivities considering 50:50 vol.% CO_2/CH_4 and CO_2/N_2 mixtures of interest, as well as simulated mixtures of biogas (40:60 vol.% CO_2/CH_4) and flue gas (15:85 vol.% CO_2/N_2). These selectivities were determined by Eqs. (4) and (5), using the parameters presented in Table S9 (See SI). In general, all composites were more selective than ZIF-8 (exception made for 15%[C_6MIM][$B(CN)_4$]@ZIF-8 on the 15:85 vol.% CO_2/N_2 mixture). For each cyano-based IL@ZIF-8 composite, CO_2/CH_4 and CO_2/N_2 selectivities increase with a higher IL loading. However, except for the 15:85 vol.% CO_2/N_2 mixture, there was a slight decrease in the selectivity with the increase of pressure. This trend is in accordance with other reported studies regarding IL@ZIF-8 composites [22,29].

The prepared composite-derived carbon materials presented higher CO_2, CH_4, and N_2 uptakes than cyano-based IL@ZIF-8 composites, but this tendency was not observed regarding the selectivities. The carbon materials showed comparable selectivities to their precursors, except in the case of the 15:85 vol.% CO_2/N_2 mixture, where a more distinguished increase in the selectivity was observed. In fact, for all mixtures, the produced carbon materials showed similar selectivities, with a decreasing tendency following the increase of the pressure. Different from cyano-based composites in relation to ZIF-8, their derived carbons were less selective

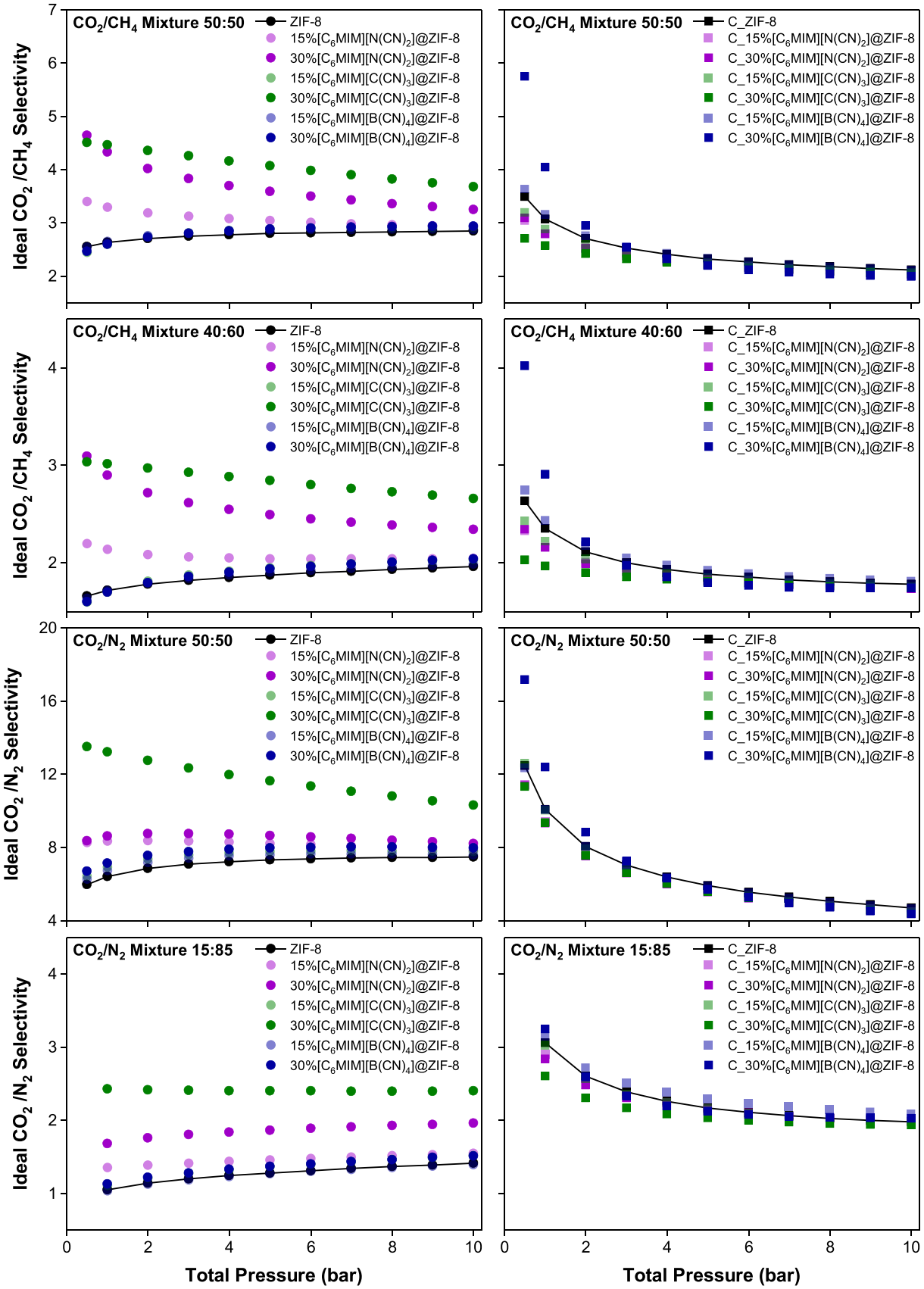

Fig. 6. Ideal CO_2/CH_4 and CO_2/N_2 selectivities for the pristine ZIF-8, cyano-based IL@ZIF-8 composites (on the left), and their respective derived carbons (on the right) as a function of total pressure, determined from the Sips isotherm model fitting of the single-component sorption-desorption isotherms measured at 303 K and in the pressure range of 0.5–16 bar.

than their counterpart C_ZIF-8. Still, C_15%[C_6MIM][$B(CN)_4$]@ZIF-8 is equally or more selective than C_ZIF-8 in all pressure range and C_30%[C_6MIM][$B(CN)_4$]@ZIF-8 is as well up to 1 bar, both for all considered mixtures. For these two materials, the selectivity is probably ascribed to their N content, which might facilitate the interaction between the sorbent surface and CO_2 molecules [43,44]. The above-mentioned results in the CO_2/CH_4 and CO_2/N_2 separation performance illustrate that composites have potential for the CO_2 separation from the flue gas (1 bar of total pressure for 15:85 vol% CO_2/N_2). The carbon materials, and mainly those derived from [C_6MIM][$B(CN)_4$]@ZIF-8 composites, can be considered promising alternative adsorbents for the same application.

4. Conclusions

In this work, the sorption capacity and selectivity performance toward CO_2 separation applications were evaluated over the composites obtained by the incorporation of three different cyano-based ILs into ZIF-8 and their respective carbon materials.

Independently of the loading, ILs were successfully impregnated into ZIF-8, preserving its structure and morphology. The composites became more selective than ZIF-8, despite the decrease of the total pore volume with the increase of the IL loading and the number of cyano groups. The selectivity increases up to 151% were observed in composites between 0 and 1 bar, depending on the considered mixture. The sorption capacity was negatively affected by the increase of the IL loading.

The high number of cyano groups in the IL anion led to composite-derived carbons with a similar or higher N content than C_ZIF-8. The ZIF-8- and composite-derived carbon materials presented ultramicropores, which explains the higher gas sorption capacity at low pressures, when compared to their precursors. At moderate-to-high pressures, the CO_2 uptake showed almost a linear dependence with the pore volume, and composite-derived carbons could not outperform C_ZIF-8 in the gas uptake.

Ideal CO_2/CH_4 and CO_2/N_2 selectivities of composites-derived carbon materials revealed the selectivity increases up to 65% between 0 and 1 bar, depending on the mixture. Their selectivity performance indicates that these materials are promising for post-combustion CO_2 separation.

Author statement

Laura M. Esteves: methodology, investigation, writing – original draft, and writing – review and editing.

Tiago J. Ferreira: methodology, investigation, writing – original draft, and writing – review and editing.

Anastasiia Keba: methodology and investigation.

José M. S. S. Esperança: conceptualization, methodology, writing – review and editing, supervision, project administration, and funding acquisition.

Isabel A.A.C. Esteves: conceptualization, methodology, writing – review and editing, supervision, project administration, and funding acquisition.

Declaration of competing interest

The authors declare that they have no known competing financial interests or personal relationships that could have appeared to influence the work reported in this paper.

Data availability

Data will be made available on request.

Acknowledgments

The authors thank Fundação para a Ciência e Tecnologia, FCT/MCTES (Portugal) for financial support through grant SFRH/BD/139627/2018 (T. J. Ferreira) and project PTDC/CTM-CTM/30326/2017. Additionally, this work was partially supported by the Associate Laboratory for Green Chemistry, LAQV, which is funded by national funds from FCT/MCTES (UIDB/50006/2020, UIDP/50006/2020 and LA/P/0008/2020).

Appendix A. Supplementary data

Supplementary data to this article can be found online at https://doi.org/10.1016/j.mtsust.2023.100353.

References

[1] N.M. Dowell, P.S. Fennell, N. Shah, G.C. Maitland, The role of CO_2 capture and utilization in mitigating climate change, Nat. Clim. Chang. 7 (2017) 243–249, https://doi.org/10.1038/nclimate3231.
[2] R.B. Jackson, C. Le Quéré, R.M. Andrew, J.G. Canadell, G.P. Peters, J. Roy, et al., Warning signs for stabilizing global CO2 emissions, Environ. Res. Lett. 12 (2017) 110202–110204, https://doi.org/10.1088/1748-9326/aa9662.
[3] S. Nabernegg, B. Bednar-Friedl, P. Muñoz, M. Titz, J. Vogel, National policies for global emission reductions: effectiveness of carbon emission reductions in international supply chains, Ecol. Econ. 158 (2019) 146–157, https://doi.org/10.1016/j.ecolecon.2018.12.006.
[4] UNFCCC, Adoption of the Paris Agreement, United Nations Framework Convention on Climate Change, Paris, 2015.
[5] REN21, Renewables 2018, Global Status Report, Paris, 2018.
[6] I. Angelidaki, L. Treu, P. Tsapekos, G. Luo, S. Campanaro, H. Wenzel, et al., Biogas upgrading and utilization: current status and perspectives, Biotechnol. Adv. 36 (2018) 452–466, https://doi.org/10.1016/j.biotechadv.2018.01.011.
[7] S. Achinas, G.J. Willem Euverink, Rambling facets of manure-based biogas production in Europe: a briefing, Renew. Sustain. Energy Rev. 119 (2020), 109566, https://doi.org/10.1016/j.rser.2019.109566.
[8] E. Blomen, C. Hendriks, F. Neele, Capture technologies: improvements and promising developments, Energy Proc. 1 (2009) 1505–1512, https://doi.org/10.1016/j.egypro.2009.01.197.
[9] W.L. Theo, J.S. Lim, H. Hashim, A.A. Mustaffa, W.S. Ho, Review of pre-combustion capture and ionic liquid in carbon capture and storage, Appl. Energy 183 (2016) 1633–1663, https://doi.org/10.1016/j.apenergy.2016.09.103.
[10] D.Y.C. Leung, G. Caramanna, M.M. Maroto-Valer, An overview of current status of carbon dioxide capture and storage technologies, Renew. Sustain. Energy Rev. 39 (2014) 426–443, https://doi.org/10.1016/j.rser.2014.07.093.
[11] J. Singh, D.W. Dhar, Overview of carbon capture technology: microalgal biorefinery concept and state-of-the-art, Front. Mar. Sci. 6 (2019) 1–9, https://doi.org/10.3389/fmars.2019.00029.
[12] F. Raganati, F. Miccio, P. Ammendola, Adsorption of carbon dioxide for post-combustion capture: a review, Energy Fuels 35 (2021) 12845–12868, https://doi.org/10.1021/acs.energyfuels.1c01618.
[13] M. Bui, C.S. Adjiman, A. Bardow, E.J. Anthony, A. Boston, S. Brown, et al., Carbon capture and storage (CCS): the way forward, Energy Environ. Sci. 11 (2018) 1062–1176, https://doi.org/10.1039/c7ee02342a.
[14] B.C.R. Camacho, R.P.P.L. Ribeiro, I.A.A.C. Esteves, J.P.B. Mota, Adsorption equilibrium of carbon dioxide and nitrogen on the MIL-53 (Al) metal organic framework, Sep. Purif. Technol. 141 (2015) 150–159, https://doi.org/10.1016/j.seppur.2014.11.040.
[15] J.L.C. Rowsell, O.M. Yaghi, Metal-organic frameworks: a new class of porous materials, Microporous Mesoporous Mater. 73 (2004) 3–14, https://doi.org/10.1016/j.micromeso.2004.03.034.
[16] K. Shen, L. Zhang, X. Chen, L. Liu, D. Zhang, Y. Han, et al., Ordered macro-microporous metal-organic framework single crystals, Science (1979) 359 (2018) 206–210, https://doi.org/10.1126/science.aao3403.
[17] H. Furukawa, K.E. Cordova, M. O'Keeffe, O.M. Yaghi, The chemistry and applications of metal-organic frameworks, Science (1979) (2013) 341, https://doi.org/10.1126/science.1230444.
[18] M. Ding, R.W. Flaig, H.L. Jiang, O.M. Yaghi, Carbon capture and conversion using metal-organic frameworks and MOF-based materials, Chem. Soc. Rev. 48 (2019) 2783–2828, https://doi.org/10.1039/c8cs00829a.
[19] H. Li, K. Wang, Y. Sun, C.T. Lollar, J. Li, H. Zhou, Recent advances in gas storage and separation using metal–organic frameworks, Mater. Today 21 (2018) 108–121, https://doi.org/10.1016/j.mattod.2017.07.006.
[20] J. Yu, L.H. Xie, J.R. Li, Y. Ma, J.M. Seminario, P.B. Balbuena, CO2 capture and separations using MOFs: computational and experimental studies, Chem. Rev. 117 (2017) 9674–9754, https://doi.org/10.1021/acs.chemrev.6b00626.
[21] I. Ahmed, S.H. Jhung, Composites of metal-organic frameworks: preparation and application in adsorption, Mater. Today 17 (2014) 136–146, https://doi.org/10.1016/j.mattod.2014.03.002.

[22] T. Ferreira, R. Pedro Pinto Lopes Ribeiro, P.B. Mota J, N. Paulo, L. Rebelo, M.S.S. Esperança J, A.A.C. Esteves I, Ionic liquid-impregnated metal-organic frameworks for CO2/CH4 separation, ACS Appl. Nano Mater. 2 (2019) 7933–7950, https://doi.org/10.1021/acsanm.9b01936.
[23] F.P. Kinik, C. Altintas, V. Balci, B. Koyuturk, A. Uzun, S. Keskin, [BMIM][PF6] incorporation doubles CO2 selectivity of ZIF-8: elucidation of interactions and their consequences on performance, ACS Appl. Mater. Interfaces 8 (2016) 30992–31005, https://doi.org/10.1021/acsami.6b11087.
[24] S. Kavak, H.M. Polat, H. Kulak, S. Keskin, A. Uzun, MIL-53(Al) as a versatile platform for ionic-liquid/MOF composites to enhance CO2 selectivity over CH4 and N2, Chem. Asian J. 14 (2019) 3655–3667, https://doi.org/10.1002/asia.201900634.
[25] T.J. Ferreira, B.A. de Moura, L.M. Esteves, P.M. Reis, J.M.S.S. Esperança, I.A.A.C. Esteves, Biocompatible ammonium-based ionic liquids/ZIF-8 composites for CO_2/CH_4 and CO_2/N_2 separations, Sustain. Mater. Technol. (2023), e00558.
[26] K. Fujie, H. Kitagawa, Ionic liquid transported into metal-organic frameworks, Coord. Chem. Rev. 307 (2016) 382–390, https://doi.org/10.1016/j.ccr.2015.09.003.
[27] F.P. Kinik, A. Uzun, S. Keskin, Ionic liquid/metal–organic framework composites: from synthesis to applications, ChemSusChem 10 (2017) 2842–2863, https://doi.org/10.1002/cssc.201700716.
[28] Y. Ban, Z. Li, Y. Li, Y. Peng, H. Jin, W. Jiao, et al., Confinement of ionic liquids in nanocages: tailoring the molecular sieving properties of ZIF-8 for membrane-based CO2 capture, Angew. Chem. Int. Ed. 54 (2015) 15483–15487, https://doi.org/10.1002/anie.201505508.
[29] M. Mohamedali, H. Ibrahim, A. Henni, Incorporation of acetate-based ionic liquids into a zeolitic imidazolate framework (ZIF-8) as efficient sorbents for carbon dioxide capture, Chem. Eng. J. 334 (2018) 817–828, https://doi.org/10.1016/j.cej.2017.10.104.
[30] S. Zeng, X. Zhang, L. Bai, X. Zhang, H. Wang, J. Wang, et al., Ionic-liquid-based CO_2 capture systems: structure, interaction and process, Chem. Rev. 117 (2017) 9625–9673, https://doi.org/10.1021/acs.chemrev.7b00072.
[31] Z. Lei, B. Chen, Y.M. Koo, D.R. Macfarlane, Introduction: ionic liquids, Chem. Rev. 117 (2017) 6633–6635, https://doi.org/10.1021/acs.chemrev.7b00246.
[32] X. Zhang, X. Zhang, H. Dong, Z. Zhao, S. Zhang, Y. Huang, Carbon capture with ionic liquids: overview and progress, Energy Environ. Sci. 5 (2012) 6668–6681, https://doi.org/10.1039/c2ee21152a.
[33] J. Hwang, A. Ejsmont, R. Freund, J. Goscianska, B.V.K.J. Schmidt, S. Wuttke, Controlling the morphology of metal-organic frameworks and porous carbon materials: metal oxides as primary architecture-directing agents, Chem. Soc. Rev. 49 (2020) 3348–3422, https://doi.org/10.1039/c9cs00871c.
[34] Q. Wu, J. Liang, J.D. Yi, D.L. Meng, P.C. Shi, Y.B. Huang, et al., Unraveling the relationship between the morphologies of metal-organic frameworks and the properties of their derived carbon materials, Dalton Trans. 48 (2019) 7211–7217, https://doi.org/10.1039/c8dt04941f.
[35] S. Ma, G.A. Goenaga, A.V. Call, D.J. Liu, Cobalt imidazolate framework as precursor for oxygen reduction reaction electrocatalysts, Chem. Eur. J. 17 (2011) 2063–2067, https://doi.org/10.1002/chem.201003080.
[36] S. Lim, K. Suh, Y. Kim, M. Yoon, H. Park, D.N. Dybtsev, et al., Porous carbon materials with a controllable surface area synthesized from metal-organic frameworks, Chem. Commun. 48 (2012) 7447–7449, https://doi.org/10.1039/c2cc33439a.
[37] B.N. Bhadra, A. Vinu, C. Serre, S.H. Jhung, MOF-derived carbonaceous materials enriched with nitrogen: preparation and applications in adsorption and catalysis, Mater. Today 25 (2019) 88–111, https://doi.org/10.1016/j.mattod.2018.10.016.
[38] B. Liu, H. Shioyama, T. Akita, Q. Xu, Metal-organic framework as a template for porous carbon synthesis, J. Am. Chem. Soc. 130 (2008) 5390–5391, https://doi.org/10.1021/ja7106146.
[39] S. Gadipelli, Z.X. Guo, Tuning of ZIF-derived carbon with high activity, nitrogen functionality, and yield – a case for superior CO2 capture, ChemSusChem 8 (2015) 2123–2132, https://doi.org/10.1002/cssc.201403402.
[40] T. Wang, H.K. Kim, Y. Liu, W. Li, J.T. Griffiths, Y. Wu, et al., Bottom-up formation of carbon-based structures with multilevel hierarchy from MOF-guest polyhedra, J. Am. Chem. Soc. 140 (2018) 6130–6136, https://doi.org/10.1021/jacs.8b02411.
[41] D.M. Reinoso, U. Diaz, M.A. Frechero, Structural study of functional hierarchical porous carbon synthesized from metal-organic framework template, Mater. Today Chem. 14 (2019), 100188, https://doi.org/10.1016/j.mtchem.2019.08.007.
[42] S. Mo, Z. Sun, X. Huang, W. Zou, J. Chen, D. Yuan, Synthesis, characterization and supercapacitive properties of hierarchical porous carbons, Synth. Met. 162 (2012) 85–88, https://doi.org/10.1016/j.synthmet.2011.11.015.
[43] W. Xing, C. Liu, Z. Zhou, L. Zhang, J. Zhou, S. Zhuo, et al., Superior CO2 uptake of N-doped activated carbon through hydrogen-bonding interaction, Energy Environ. Sci. 5 (2012) 7323–7327, https://doi.org/10.1039/c2ee21653a.
[44] F. Sun, X. Liu, J. Gao, X. Pi, L. Wang, Z. Qu, et al., Highlighting the role of nitrogen doping in enhancing CO2 uptake onto carbon surface: a combined experimental and computational analysis, J. Mater. Chem. A Mater. 4 (2016) 18248–18252, https://doi.org/10.1039/C6TA08262A.
[45] A. Aijaz, T. Akita, H. Yang, Q. Xu, From ionic-liquid@metal-organic framework composites to heteroatom-decorated large-surface area carbons: superior CO2 and H2 uptake, Chem. Commun. 50 (2014) 6498–6501, https://doi.org/10.1039/c4cc02459a.
[46] S. Zhang, K. Dokko, M. Watanabe, Carbon materialization of ionic liquids: from solvents to materials, Mater. Horiz. 2 (2015) 168–197, https://doi.org/10.1039/c4mh00141a.
[47] Z.L. Xie, D.S. Su, Ionic liquid based approaches to carbon materials synthesis, Eur. J. Inorg. Chem. 2015 (2015) 1137–1147, https://doi.org/10.1002/ejic.201402607.
[48] J.H. Jeong, J.S. Lee, K.C. Roh, K. Kim, Multimodal porous carbon derived from ionic liquids: correlation between pore sizes and ionic clusters, Nanoscale 9 (2017) 14672–14681, https://doi.org/10.1039/c7nr05647h.
[49] X. Zhu, P.C. Hillesheim, S.M. Mahurin, C. Wang, C. Tian, S. Brown, et al., Efficient CO2 capture by porous, nitrogen-doped carbonaceous adsorbents derived from task-specific ionic liquids, ChemSusChem 5 (2012) 1912–1917, https://doi.org/10.1002/cssc.201200355.
[50] A. Aijaz, T. Akita, H. Yang, Q. Xu, From ionic-liquid@metal-organic framework composites to heteroatom-decorated large-surface area carbons: superior CO2 and H2 uptake, Chem. Commun. 50 (2014) 6498–6501, https://doi.org/10.1039/c4cc02459a.
[51] S.M. Mahurin, P.F. Fulvio, P.C. Hillesheim, K.M. Nelson, G.M. Veith, S. Dai, Directed synthesis of nanoporous carbons from task-specific ionic liquid precursors for the adsorption of CO2, ChemSusChem 7 (2014) 3284–3289, https://doi.org/10.1002/cssc.201402338.
[52] S. Zhang, K. Dokko, M. Watanabe, Direct synthesis of nitrogen-doped carbon materials from protic ionic liquids and protic salts: structural and physicochemical correlations between precursor and carbon, Chem. Mater. 26 (2014) 2915–2926, https://doi.org/10.1021/cm5006168.
[53] M. Sarker, H.J. An, D.K. Yoo, S.H. Jhung, Nitrogen-doped porous carbon from ionic liquid@Al-metal-organic framework: a prominent adsorbent for purification of both aqueous and non-aqueous solutions, Chem. Eng. J. 338 (2018) 107–116, https://doi.org/10.1016/j.cej.2017.12.157.
[54] M. Sarker, I. Ahmed, S.H. Jhung, Adsorptive removal of herbicides from water over nitrogen-doped carbon obtained from ionic liquid@ZIF-8, Chem. Eng. J. 323 (2017) 203–211, https://doi.org/10.1016/j.cej.2017.04.103.
[55] I. Ahmed, T. Panja, N.A. Khan, M. Sarker, J.S. Yu, S.H. Jhung, Nitrogen-doped porous carbons from ionic liquids@MOF: remarkable adsorbents for both aqueous and nonaqueous media, ACS Appl. Mater. Interfaces 9 (2017) 10276–10285, https://doi.org/10.1021/acsami.7b00859.
[56] B.N. Bhadra, H.J. Lee, S.H. Jhung, Adsorptive removal of herbicides with similar structures from water over nitrogen-enriched carbon, derived from melamine@metal-azolate framework-6, Environ. Res. 204 (2021), 111991, https://doi.org/10.1016/j.envres.2021.111991.
[57] D.D. Do, Adsorption Analysis: Equilibria and Kinetics, Imperial College Press, 1998.
[58] J. Landers, Gor Gyu, A. v. Neimark, Density functional theory methods for characterization of porous materials, Colloids Surf. A Physicochem. Eng. Asp. 437 (2013) 3–32, https://doi.org/10.1016/j.colsurfa.2013.01.007.
[59] I.A.A.C. Esteves, M.S.S. Lopes, P.M.C. Nunes, J.P.B. Mota, Adsorption of natural gas and biogas components on activated carbon, Sep. Purif. Technol. 62 (2008) 281–296, https://doi.org/10.1016/j.seppur.2008.01.027.
[60] S. Gumma, O. Talu, Net adsorption: a thermodynamic framework for supercritical gas adsorption and storage in porous solids, Langmuir 26 (2010) 17013–17023, https://doi.org/10.1021/la102186q.
[61] T.J. Ferreira, L.M. Esteves, J.M.S.S. Esperança, I.A.A.C. Esteves, Unveiling the temperature influence on the sorptive behaviour of ZIF-8 composite materials impregnated with [CnMIM][$B(CN)_4$] ionic liquids, Processes 10 (2022) 247, https://doi.org/10.3390/pr10020247.
[62] J.B. James, Y.S. Lin, Kinetics of ZIF-8 Thermal Decomposition in Inert, Oxidizing, and Reducing Environments, 2016, https://doi.org/10.1021/acs.jpcc.6b01208.
[63] M.B. Meredith, C.H. McMillen, J.T. Goodman, T.P. Hanusa, Ambient temperature imidazolium-based ionic liquids with tetrachloronickelate(II) anions, Polyhedron 28 (2009) 2355–2358, https://doi.org/10.1016/j.poly.2009.04.037.
[64] T.P. Fellinger, D.S. Su, M. Engenhorst, D. Gautam, R. Schlögl, M. Antonietti, Thermolytic synthesis of graphitic boron carbon nitride from an ionic liquid precursor: mechanism, structure analysis and electronic properties, J. Mater. Chem. 22 (2012) 23996–24005, https://doi.org/10.1039/c2jm34486f.
[65] F.P. Kinik, C. Altintas, V. Balci, B. Koyuturk, A. Uzun, S. Keskin, [BMIM][PF_6] incorporation doubles CO_2 selectivity of ZIF-8: elucidation of interactions and their consequences on performances, ACS Appl. Mater. Interfaces 8 (2016) 30992–31005, https://doi.org/10.1021/acsami.6b11087.
[66] M. Zeeshan, K. Yalcin, F.E. Sarac Oztuna, U. Unal, S. Keskin, A. Uzun, A new class of porous materials for efficient CO2 separation: ionic liquid/graphene aerogel composites, Carbon N. Y. 171 (2021) 79–87, https://doi.org/10.1016/j.carbon.2020.08.079.
[67] B. Koyuturk, C. Altintas, F.P. Kinik, S. Keskin, A. Uzun, Improving gas separation performance of ZIF-8 by [BMIM][BF4] incorporation: interactions and their consequences on performance, J. Phys. Chem. C 121 (2017) 10370–10381, https://doi.org/10.1021/acs.jpcc.7b00848.
[68] T.J. Ferreira, A.T. Vera, BA De Moura, L.M. Esteves, M. Tariq, J.M.S.S. Esperança, et al., Paramagnetic ionic liquid/metal organic framework composites for CO2/CH4 and CO2/N2 separations, Front. Times 8 (2020) 1087, https://doi.org/10.3389/fchem.2020.590191.
[69] L.C. Tomé, M. Isik, C.S.R. Freire, D. Mecerreyes, I.M. Marrucho, Novel pyrrolidinium-based polymeric ionic liquids with cyano counter-anions: HIGH performance membrane materials for post-combustion CO2

separation, J. Memb. Sci. 483 (2015) 155–165, https://doi.org/10.1016/j.memsci.2015.02.020.
[70] X. Ma, L. Li, S. Wang, M. Lu, H. Li, W. Ma, et al., Ammonia-treated porous carbon derived from ZIF-8 for enhanced CO2 adsorption, Appl. Surf. Sci. 369 (2016) 390–397, https://doi.org/10.1016/j.apsusc.2016.01.274.
[71] Z. Abbasi, E. Shamsaei, S.K. Leong, B. Ladewig, X. Zhang, H. Wang, Effect of carbonization temperature on adsorption property of ZIF-8 derived nanoporous carbon for water treatment, Microporous Mesoporous Mater. 236 (2016) 28–37, https://doi.org/10.1016/j.micromeso.2016.08.022.
[72] R.P.P.L. Ribeiro, C.L. Antunes, A.U. Garate, A.F. Portela, M.G. Plaza, J.P.B. Mota, et al., Binderless shaped metal-organic framework particles: impact on carbon dioxide adsorption, Microporous Mesoporous Mater. 275 (2019) 111–121, https://doi.org/10.1016/j.micromeso.2018.08.002.
[73] H.M. Polat, S. Kavak, H. Kulak, A. Uzun, S. Keskin, CO2 separation from flue gas mixture using [BMIM][BF4]/MOF composites: linking high-throughput computational screening with experiments, Chem. Eng. J. 394 (2020), https://doi.org/10.1016/j.cej.2020.124916.
[74] M. Thommes, K. Kaneko, A.V. Neimark, J.P. Olivier, F. Rodriguez-reinoso, J. Rouquerol, et al., Physisorption of gases , with special reference to the evaluation of surface area and pore size distribution (IUPAC Technical Report), Pure Appl. Chem. 87 (2015) 1051–1069, https://doi.org/10.1515/pac-2014-1117.
[75] S. Zhang, K. Dokko, M. Watanabe, Direct synthesis of nitrogen-doped carbon materials from protic ionic liquids and protic salts: structural and physicochemical correlations between precursor and carbon, Chem. Mater. 26 (2014) 2915–2926, https://doi.org/10.1021/cm5006168.
[76] Y.C. Chiang, C.Y. Yeh, C.H. Weng, Carbon dioxide adsorption on porous and functionalized activated carbon fibers, Appl. Sci. 9 (2019), https://doi.org/10.3390/app9101977.
[77] Q. Guo, C. Chen, Z. Li, X. Li, H. Wang, N. Feng, et al., Controllable construction of N-enriched hierarchically porous carbon nanosheets with enhanced performance for CO2 capture, Chem. Eng. J. 371 (2019) 414–423, https://doi.org/10.1016/j.cej.2019.04.062.
[78] S. Kayal, A. Chakraborty, Activated carbon (type Maxsorb-III) and MIL-101(Cr) metal organic framework based composite adsorbent for higher CH_4 storage and CO_2 capture, Chem. Eng. J. 334 (2018) 780–788, https://doi.org/10.1016/j.cej.2017.10.080.
[79] F. Dreisbach, R. Staudt, J.U. Keller, High pressure adsorption data of methane, nitrogen, carbon dioxide and their binary and ternary mixtures on activated carbon, Adsorption 5 (1999) 215–227, https://doi.org/10.1023/A:1008914703884.
[80] J.A. Delgado, V.I. Águeda, M.A. Uguina, J.L. Sotelo, P. Brea, C.A. Grande, Adsorption and diffusion of H_2, CO, CH_4, and CO_2 in BPL activated carbon and 13X zeolite: evaluation of performance in pressure swing adsorption hydrogen purification by simulation, Ind. Eng. Chem. Res. 53 (2014) 15414–15426, https://doi.org/10.1021/ie403744u.
[81] Y. He, J.-H. Yun, N.A. Seaton, Adsorption equilibrium of binary methane/ethane mixtures in BPL activated carbon: isotherms and calorimetric heats of adsorption, Langmuir 20 (2004) 6668–6678, https://doi.org/10.1021/la036430v.
[82] I.A.A.C. Esteves, M.S.S. Lopes, P.M.C. Nunes, J.P.B. Mota, Adsorption of natural gas and biogas components on activated carbon, Sep. Purif. Technol. 62 (2008) 281–296, https://doi.org/10.1016/j.seppur.2008.01.027.
[83] E. Surra, R.P.P.L. Ribeiro, T. Santos, M. Bernardo, J.P.B. Mota, N. Lapa, et al., Evaluation of activated carbons produced from Maize Cob Waste for adsorption-based CO_2 separation and biogas upgrading, J. Environ. Chem. Eng. 10 (2022), 107065, https://doi.org/10.1016/j.jece.2021.107065.